



HAL
open science

Compaction of Duplex Nucleic Acids upon Native Electrospray Mass Spectrometry

Massimiliano Porrini, Frédéric Rosu, Clémence Rabin, Leonardo Darré,
Hansel Gómez, Modesto Orozco, Valérie Gabelica

► **To cite this version:**

Massimiliano Porrini, Frédéric Rosu, Clémence Rabin, Leonardo Darré, Hansel Gómez, et al.. Compaction of Duplex Nucleic Acids upon Native Electrospray Mass Spectrometry. ACS Central Science, 2017, 3 (5), pp.454-461. 10.1021/acscentsci.7b00084 . hal-04127049

HAL Id: hal-04127049

<https://hal.science/hal-04127049>

Submitted on 13 Jun 2023

HAL is a multi-disciplinary open access archive for the deposit and dissemination of scientific research documents, whether they are published or not. The documents may come from teaching and research institutions in France or abroad, or from public or private research centers.

L'archive ouverte pluridisciplinaire **HAL**, est destinée au dépôt et à la diffusion de documents scientifiques de niveau recherche, publiés ou non, émanant des établissements d'enseignement et de recherche français ou étrangers, des laboratoires publics ou privés.

Compaction of Duplex Nucleic Acids upon Native Electrospray Mass Spectrometry

Massimiliano Porrini,[†] Frédéric Rosu,[‡] Clémence Rabin,[†] Leonardo Darré,^{§,||} Hansel Gómez,^{§,||} Modesto Orozco,^{§,||,⊥} and Valérie Gabelica^{*,†,||}

[†]INSERM, CNRS, Université de Bordeaux, Acides Nucléiques Régulations Naturelle et Artificielle (ARNA, U1212, UMR5320), IECB, 2 rue Robert Escarpit, 33607 Pessac, France

[‡]CNRS, INSERM, Université de Bordeaux, Institut Européen de Chimie et Biologie (IECB, UMS3033, US001), 2 rue Robert Escarpit, 33607 Pessac, France

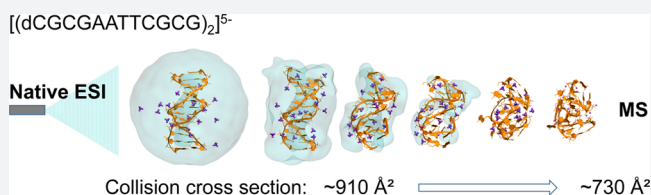
[§]The Barcelona Institute of Science and Technology, Institute for Research in Biomedicine (IRB) Barcelona, Baldiri Reixac 10, 08028 Barcelona, Spain

^{||}Joint BSC-CRG-IRB Research Program in Computational Biology, IRB Barcelona, Barcelona, Spain

[⊥]Department of Biochemistry and Biomedicine, University of Barcelona, Avda Diagonal 647, 08028 Barcelona, Spain

Supporting Information

ABSTRACT: We report on the fate of nucleic acids conformation in the gas phase as sampled using native mass spectrometry coupled to ion mobility spectrometry. On the basis of several successful reports for proteins and their complexes, the technique has become popular in structural biology, and the conformation survival becomes more and more taken for granted. Surprisingly, we found that DNA and RNA duplexes, at the electrospray charge states naturally obtained from native solution conditions (≥ 100 mM aqueous NH_4OAc), are significantly more compact in the gas phase compared to the canonical solution structures. The compaction is observed for all duplex sizes (gas-phase structures are more compact than canonical B-helices by $\sim 20\%$ for 12-bp, and by up to $\sim 30\%$ for 36-bp duplexes), and for DNA and RNA alike. Molecular modeling (density functional calculations on small helices, semiempirical calculations on up to 12-bp, and molecular dynamics on up to 36-bp duplexes) demonstrates that the compaction is due to phosphate group self-solvation prevailing over Coulomb repulsion. Molecular dynamics simulations starting from solution structures do not reproduce the experimental compaction. To be experimentally relevant, molecular dynamics sampling should reflect the progressive structural rearrangements occurring during desolvation. For nucleic acid duplexes, the compaction observed for low charge states results from novel phosphate–phosphate hydrogen bonds formed across both grooves at the very late stages of electrospray.



■ INTRODUCTION

Besides genetic information storage, nucleic acids perform pivotal regulatory functions in living organisms.¹ Conformational changes are key to these regulation mechanisms, whether at the DNA level (e.g., particular structures in gene promoters)² or at the RNA level (e.g., riboswitches).³ There is thus a need for new experimental approaches enabling one to detect and characterize the different ensembles of conformation simultaneously present in solution. “Native” electrospray ionization mass spectrometry (ESI-MS) helps to decipher the complexation equilibria.^{4–7} “Native MS” means that the solution conditions must be compatible with electrospray ionization, yet allow the system to fold in the same way as it would in physiological conditions.⁸ The typical solution condition for native MS is aqueous ammonium acetate (neutral pH, no organic cosolvent). Also, the mass spectrometer must be operated in “soft” conditions, meaning that the internal energy imparted to the ions must be just enough to desolvate the biomolecules and strip nonspecific ionic adducts,

but not too high so as not to disrupt the complexes before they reach the mass analyzer.

Ion mobility spectrometry (IMS) further enables characterization of the shape of each complex separated by mass, based on the electrophoretic mobility of the ions in a buffer gas.⁹ Coupled to ion mobility spectrometry (IMS), native mass spectrometry thus makes it possible to reveal the topology of multi-protein complexes,¹⁰ conformational changes upon ligand binding,^{11–13} or the architecture of synthetic supramolecular assemblies.¹⁴ But before native ESI-IMS-MS can be applied to characterize nucleic acids conformations in solution, it is essential to understand to what extent the different types of DNA/RNA secondary structures are preserved, or affected, by the transition from the solution to the gas phase.

Tandem mass spectrometry^{15–18} experiments have shown that the kinetic stability of gas-phase DNA duplexes was

Received: February 22, 2017

Published: April 26, 2017

correlated with the fraction of guanine–cytosine (GC) base pairs and with the base pair ordering. This suggested that Watson–Crick (WC) hydrogen bonding and base stacking were at least partially maintained in the gas phase. Infrared multiphoton dissociation spectroscopy on duplexes and single strands suggested that GC bases are engaged in hydrogen bonds in the gas-phase duplexes, although no such evidence was found for AT base pairs.¹⁹ Early molecular dynamics (MD) validated this view: although (12-mer)₂⁶⁻ and (16-mer)₂⁸⁻ duplexes were distorted in the gas phase, most WC H-bonding and stacking interactions were preserved, particularly in GC-rich regions.²⁰

The Bowers group further explored the gas-phase structure of DNA duplexes by IMS.^{21,22} By comparing the experimental collision cross section (CCS) of d(GC)_n duplexes with those obtained on duplexes relaxed by short (5 ns) MD, they showed that the gas-phase structures resemble an A-helix for the short duplexes (8–16-mer) and a B-helix for longer ones (>18-mer). However, those experiments had been performed on the relatively high charge states (1 negative charge per 2 base pairs) obtained from solution conditions (49:49:2 mixture of H₂O/MeOH/NH₄OH) differing markedly from those typically used in native MS. Here we show that, at the lower charge states typically obtained from native MS conditions (100–150 mM NH₄OAc in 100% H₂O, pH = 7), the gas-phase conformations are significantly more compact than expected for B- or A-helices. We investigated the physical origin of this gas-phase compaction by molecular modeling.

RESULTS AND DISCUSSION

DNA Duplexes in Their Predominant Native Charge State Are More Compact than a Canonical B-Helix. The sequences studied here were designed based on the Dickerson–Drew dodecamer,²³ here noted 12-d₆₆ indicating the number of base pairs (12), the nucleotide type (i.e., d for DNA and r for RNA), and the GC base pair percentage content (66%) as a subscript. This notation was used throughout the text. DNA or RNA duplexes were prepared by annealing in aqueous ammonium acetate and analyzed using drift tube ion mobility in helium (see methods and Supporting Information Section S1). In aqueous NH₄OAc, RNA sequences fold into the A-form, and DNA sequences fold into the B-form (according to the circular dichroism²⁴ spectra in Supporting Information Figure S2).

When sprayed from aqueous 100 mM NH₄OAc, the major charge state of 12-bp duplexes is 5⁻ (Figure S3). This may seem at odds with the solution charge of the nucleic acid alone, which is 22⁻. One should however keep in mind that an atmosphere of counterions surrounds nucleic acids in solution.²⁵ If counterions were not present, the electrostatic repulsion between strands would amount to hundreds of kT, and double helices would not exist. The effective charge state of nucleic acids in solution is hard to define: bulk solutions being electrically neutral, the net charge of a duplex depends on which distance from the nucleic acid atoms one places the boundary. Molecular dynamics simulations on 18-bp B-DNA duplexes²⁶ showed that neutrality is reached at an average distance of 24 Å from the center of the helix, and that 76% neutralization (a threshold defined by Manning’s counterion condensation model²⁷) is reached at 18 Å. Electrospray droplets are however not neutral, and the final charge states could reflect the thickness of the layer of solvent and counterions surrounding the nucleic acid in the final droplets.

The ^{DT}CCS_{He} distributions for the 5⁻ duplexes without ammonium ions bound and in the softest ion transfer conditions are shown in Figure 1A (full results in Supporting Figure S4).

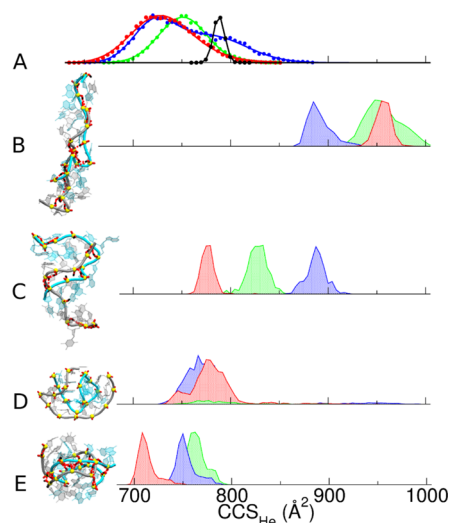


Figure 1. (A) Experimental ^{DT}CCS_{He} distribution measured under soft native conditions for the 12-bp DNA duplexes (green: (12-d₃₃)⁵⁻, blue: (12-d₆₆)⁵⁻, red: (12-d₁₀₀)⁵⁻; see Table 1 for full sequences) and the rigid G-quadruplex ([d(TG₄T)]₄)⁵⁻ (black). (B–E) Calculated CCS distributions for molecular models generated by (B) gas-phase MD of the B-helices, (C) gas-phase MD of the A-helices, (D) T-REM simulations on B-helices using distributed charges (note that most of the population of (12-d₃₃)⁵⁻ duplex dissociated during simulations), and (E) MD following a restrained minimization forcing H-bond formation between the phosphate groups across both grooves of a B-helix. The final MD structures of each duplex model, created with VMD software,²⁹ are shown for (12-d₆₆)⁵⁻ on the same scale (see Supporting Figure S11 for a magnification).

These distributions suggest more compact structures than those of canonical B- or A-forms (Table 2). Upon pre-IMS activation, the CCS distribution of 12-d₃₃ is unchanged, 12-d₆₆ is losing the high-CCS peak to the profit of the low-CCS peak, and the entire distribution of 12-d₁₀₀ is shifting toward lower CCS (from 730 Å down to ~705 Å², see Supporting Information Figure S5). At low pre-IMS activation, duplexes⁵⁻ with ammonium adducts are also detected. The CCS of these ions is similar to that of the bare duplexes, but for 12-d₆₆ the higher-CCS peak is more abundant—see Supporting Figure S6). The peak center values obtained for soft and harsh conditions are listed in Table 2. Charge states 4⁻ and 6⁻ are also detected in aqueous NH₄OAc. The duplex CCS distributions are highly charge-state dependent (see Supplementary Figure S4): charge states 4⁻ and 5⁻ are similarly compact, whereas charge state 6⁻ has a ~20% larger CCS. Charge state 7⁻, obtained for 12-d₆₆ and 12-d₁₀₀ by adding the “supercharging” agent sulfolane,²⁸ has a >30% larger CCS. The duplex CCS distributions are significantly broader than those of the tetramolecular G-quadruplex [d(TG₄T)]₄ (in black in Figure 1A, and Supplementary Figure S4), a rigid structure with the same number of bases. This indicates that a greater conformational space is explored in the gas phase by nucleic acid duplexes compared to the G-quadruplex,¹⁸ and that gas-phase duplexes consist of an ensemble of conformations not fully interconverting on the time scale of the mobility separation (10–30 ms).

MD Trajectories, DFT, and Semiempirical Optimizations Reveal Phosphate–Phosphate Hydrogen Bond Formation. To find out which three-dimensional structures are compatible with the experimental CCS values of the 12-bp⁵⁻ duplexes, we first carried out unbiased MD simulations directly from B- and A-helix structures, stripped of the solvent. The two

Table 1. Size, Name, and Sequences of the Duplexes under Study, and Outline of Calculations

size	theoretical levels of study for each size	name	sequence
10 bp	DFT (M06-2X - 4-31G(d)) semiempirical (PM7)	10-bp	dCGCGGGCCCG-dCGGGCCCGG
12 bp	semiempirical (PM7) MD from different starting structures (1 μ s each) T-REMD (1 μ s \times 18 replicas)	12-d ₃₃	(dCGTAAATTTACG) ₂
		12-d ₆₆	(dCGCGAATTCGCG) ₂
		12-d ₁₀₀	(dCGCGGGCCCGCG) ₂
		12-r ₃₃	(rCGUAAAUUUACG) ₂
		12-r ₆₆	(rCGCGAAUUCGCG) ₂
		12-r ₁₀₀	(rCGCGGGCCCGCG) ₂
24/36 bp	MD on B-helix (0.25 μ s) MD on zipped helix (0.5 μ s)	Concatenations of the 12-bp duplexes above. See Supporting Information Section S9.	

possibilities to reduce the total charge to -5 (major charge state) are the localized charges (LC) and distributed charges (DC) models.²⁰ With the DC model, the net charge of each phosphate group is reduced so that the total charge of the duplex is -5 . With the LC model, protons are added on 17 out of the 22 phosphate groups. LC and DC gave similar results upon unbiased MD of duplexes,²⁰ so here only the LC model was tested extensively.

Figure 1B,C shows representative CCS distributions. All such simulations give CCS values significantly larger than the experimental ones. Independent trajectories, started from different conformations and with different sets of localized charges, confirmed this result (Supporting Figure S8). The experimental CCS values of the duplexes⁶⁻ are nonetheless compatible with the simulated A- and B-helices, and duplexes⁷⁻ are compatible with B-helices. This does not necessarily mean that the gas-phase conformations of 6- and 7- charge states are A- and B-helices, but it helps to understand conclusions previously derived solely based on more densely charged duplexes.^{21,22}

When starting from the B-form, MD simulations always show spontaneous hydrogen bond formation between phosphate groups situated on each side of the minor groove (Supporting Information Movie S1 and Figure S9). This causes the “zipping” of the minor groove. The structures are stable up to 1 μ s (Figure S9), but too elongated compared to the duplexes⁵⁻ experimental data (compare Figure 1B with 1A). In simulations starting from the A-helix, zipping occurs as well, but this time across the major groove (Supporting Figure S10). In the gas phase, the closest protonated phosphate groups therefore tend to form hydrogen bonds that did not exist in solution. However, this kind of simulation does not reproduce the experiments.

To check for possible artifacts due to using classical force fields to represent macromolecules in the gas phase, we also studied B-duplexes at the density functional theory (DFT) and semiempirical (SE) levels. Upon DFT optimization of 7-bp to 10-bp duplexes, phosphate groups form new H-bonds and close the minor groove as well (Figure 2 and Supporting Figure S12). WC H-bonds base stacking are well preserved,^{30,31} and the helix compresses along its longitudinal axis (Figure 2C) and the $^{CALC}CCS_{He}$ of the DFT optimized structure is smaller than that of the canonical helix.

For SE calculations, we first validated that the PM7 method best reproduces the DFT results (Supporting Figure S13). The CCS values obtained after PM7 optimization are summarized in Table 2 for all [12-bp duplexes]⁵⁻ (A- and B-form for DNA and A-form for RNA). Upon PM7 optimization, the duplex [12-d₆₆]⁵⁻ undergoes minor groove zipping, while WC H-bonds and base pair stacking interactions are preserved (Figure S14). The

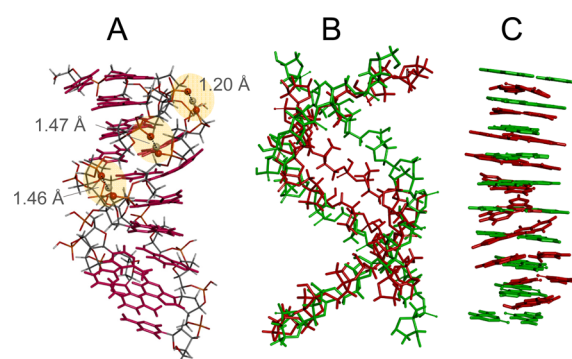


Figure 2. DFT optimization of the 10-bp duplex⁴⁻: (A) new hydrogen bonds formed between phosphate groups across the minor groove; (B) superposition of the sugar-phosphate backbones of the canonical B-helix (green) and optimized duplex (red); (C) superposition of the base pairs of the canonical B-helix (green) and optimized duplex (red).

compaction compared to the solution structure is only $\sim 8\%$, still far from the experimental value.

Thus, starting from naked canonical structures, neither geometry optimization nor unbiased MD trajectories lead the system toward the experimentally observed conformational ensemble. So, either the sampling is incomplete (simulated and experimental time scales differ), or the starting structures, obtained by desolvating and charging the duplexes all at once, inadequately reflect the electrospray droplet desolvation and declustering.

Temperature Replica Exchange MD (T-REMD) Exploration of Gas-Phase Conformational Landscapes Do Not Converge to the Experimental Structure. To enhance sampling, we carried out T-REMD simulations on the 12-bp duplexes⁵⁻ starting from their canonical structures. Because temperature replica exchange MD (T-REMD) simulations on gas-phase duplexes have never been attempted before, LC and DC models were both tested for T-REMD. DNA and RNA results, including representative snapshots, total hydrogen bonding, WC hydrogen bonding and stacking³² occupancies, are summarized in Supporting Information Section S7 (Figures S15–S25). For RNA, the theoretical CCS distributions, both with the DC and LC models, match with the experimental ones (Figures S16 and S19). However, the hydrogen bonding and stacking patterns (Figures S20–S22) always become scrambled in the gas phase. For DNA, the T-REMD results depend more critically on the charge location model: $^{CALC}CCS_{He}$ values agree with the experiments for the DC model (Figure 1D) and for some LC models (Figure 3).

Table 2. Collision Cross Section Values in Helium (CCS_{He}) of 12-bp Duplexes, Experimental and Calculated Prior and Subsequent to PM7 Optimization, Unbiased MD, T-REMD (DC Model; Results with LC Model Are Not Listed Because They Depend on the Chosen Locations—See Text), and Unbiased MD on the Helix Zipped by Restrained Minimization^a

	$\text{D}^{\text{T}}\text{CCS}_{\text{He}}$ (\AA^2)	$\text{CALC}\text{CCS}_{\text{He}}$ (\AA^2)								
		B-helix				A-helix				zipped helix
		canonical	PM7	MD	T-REMD (DC)	canonical	PM7	MD	T-REMD (DC)	MD
$[12\text{-d}_{33}]^{5-}$	soft/harsh: 760	918	914	954 ± 18	780 ± 24	900	861	826 ± 11		759 ± 12
$[12\text{-d}_{66}]^{5-}$	soft: 735/803	903	831	881 ± 6	770 ± 15	893	942	886 ± 10		752 ± 10
	harsh: 735									
$[12\text{-d}_{100}]^{5-}$	soft: 730	908	838	953 ± 8	771 ± 14	892	869	774 ± 6		711 ± 9
	harsh: 705									
$[12\text{-r}_{33}]^{5-}$						944	938		741 ± 21	
$[12\text{-r}_{66}]^{5-}$	soft/harsh: 725					945	902		747 ± 18	
$[12\text{-r}_{100}]^{5-}$	soft: 735					940	896		743 ± 11	
	harsh: 695									

^aErrors reported for MD are the standard deviation on the different structures along the trajectory.

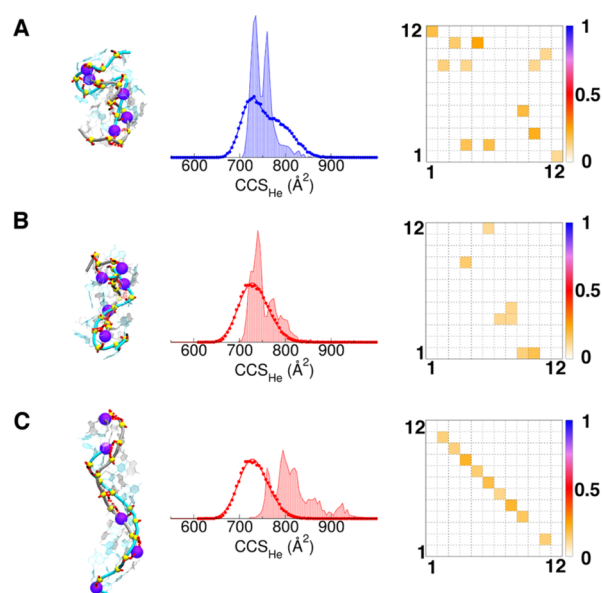


Figure 3. T-REMD on 12-bp DNA duplexes⁵⁻ with localized charges (LC). (A) $[12\text{-d}_{66}]^{5-}$, (B–C) $[12\text{-d}_{100}]^{5-}$ with different LC models. The location of negatively charged phosphates is shown by the beads on the representative snapshot structure. The experimental $\text{D}^{\text{T}}\text{CCS}_{\text{He}}$ distribution and calculated one (shade) are overlaid. The fractional WC H-bond occupancies are shown on the right: the bases of each strand are numbered from 5' to 3', and perfect base pair matching is therefore indicated by a diagonal from top left to bottom right.

With the DC model, the CCS values are closer to the experimental ones, yet still significantly too large for 12-d_{100}^{5-} . The GC base pairs are mostly preserved (Figure S37), but the duplex 12-d_{33}^{5-} is mostly melted (separated into single strands; see Figure S15). DC models lack the explicit protons and therefore cannot form phosphate–phosphate hydrogen bonds. As a result, the strands can dissociate upon T-REMD. The rate of strand dissociation occurrence ranks $12\text{-d}_{33} > 12\text{-d}_{66} > 12\text{-d}_{100}$ (Supporting Figure S15), in line with the relative gas-phase kinetic stabilities in tandem mass spectrometry.^{15–18}

When LC models are used, the T-REMD final structures depend significantly on the choice of charge location (Figure S18, S20–S22). For example, for $[12\text{-d}_{100}]^{5-}$, a first model (Figure 3B) gives CCS values matching well with the experiment, but has lost most WC H-bonds, whereas a second model (Figure

3C) preserves WC H-bonds but its CCS values are much larger than the experimental ones (the representative structure resembles those obtained with unbiased simulations starting from the B-form).

In summary, the T-REMD results do not account simultaneously for the preservation of GC base pairs and the experimental collision cross sections. Yet they teach us that the duplex⁵⁻ conformations are closer to a compact globular shape than to the helices obtained by unbiased MD trajectories and suggest that sampling problems are at least partially responsible for the lack of agreement between simulation and experimental CCSs.

Progressive Duplex Desolvation Leads to Experimentally Relevant Structures. All simulations presented to this point, and nearly all previous simulations, are assuming an instantaneous transfer of the duplex from solution to the gas phase. But in practice, desolvation and declustering proceed gradually during the experiment. Consta and co-workers³³ modeled the desolvation process of duplex $\text{dA}_{11}\text{-dT}_{11}$ at the atomistic level in a water droplet containing Na^+ and Cl^- , and found that the duplex collapses inside the droplet when the Na^+ cations are numerous enough to interact with the phosphates and reduce the size of both grooves. Interestingly, the resulting charge density is similar to that observed experimentally from native conditions. It is therefore likely that the DNA duplexes are desolvated via the charged residue model^{34,35} and that the compaction results from the association of NH_4^+ cations to both minor and major groove before full desolvation. As a result, the starting structure for gas phase simulations might be quite different from the canonical A- or B-helices. Because electrostatic interactions prevail, the gas phase conformational space is very stiff, and an incorrect starting structure can significantly bias the entire trajectory.

Here we simulated the desolvation of duplex 12-d_{66} placed in a droplet containing ~ 2400 water molecules and 17 NH_4^+ (net charge = -5). When the simulation at 350 K reaches 39.5 ns, 87 water molecules remain on the duplex together with the 17 NH_4^+ cations. The simulation was pursued for 50 ns at 450 K, to allow this ultrastable inner solvation shell of water molecules to evaporate. The ammonium ions sticking to the duplex are mainly located close to phosphate groups, often in-between them. Several trajectories (see 4–, 5–, and 6– charge states in Supporting Information Section S8; Figures S26–S31) lead to a chain of ammonium ions in the minor groove. For the 5– charge

state, ammonium ions are more distributed across both grooves, and thus upon evaporation both grooves get narrower to enable phosphate–ammonium–phosphate salt bridges to form. Accordingly, the CCS value diminishes (Figure 4).

Classical MD cannot model proton transfer, but if water evaporation is almost complete before the proton transfers start, then the structures generated by gradual desolvation are good candidates for modeling the electrosprayed structures. Also, ammonium ion positioning upon desolvation could predict which phosphate groups will share a proton and form hydrogen bonds after complete declustering.

To simulate the eventual ammonia loss, we arbitrarily transferred a proton from each ammonium ion to its closest phosphate oxygen. The resulting desolvated and declustered duplex (12-d_{66})⁵⁻ is stable over 1- μs MD at 300 K (Figure 4). The total hydrogen bond occupancy reveals additional contacts across both grooves. Remarkably, the CCS value now matches the experimental one, and at the same time, the generated structure keeps partial memory of the WC base pairs (at least, preserving mostly the GC ones), in line with CID and IRMPD results.

In summary, progressive desolvation, allowing the duplex to form phosphate-phosphate hydrogen bonds across both grooves, can account simultaneously for the experimental compactness and for partial preservation of GC base pairs. In contrast, upon unbiased MD or structure optimization (DFT or SE), only the phosphate groups that were the closest in the starting structure (across the minor and major groove for B- and A-helices, respectively) could mate.

Longer Duplexes, DNA and RNA Alike, Undergo Compaction When Electrosprayed from Aqueous Solutions of Physiological Ionic Strength. Past studies on GC-

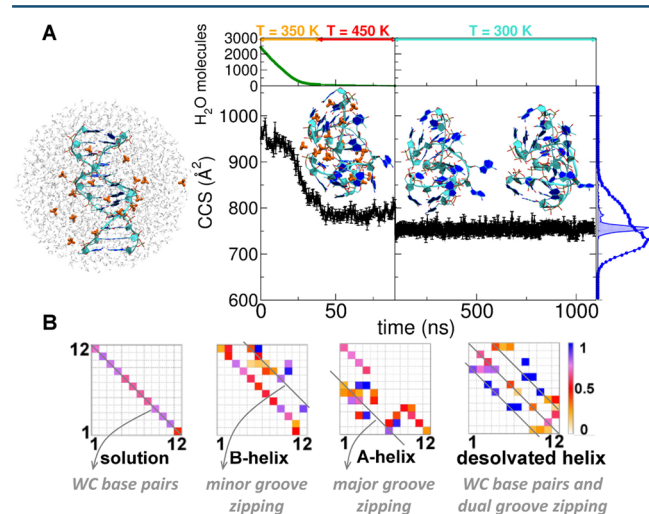


Figure 4. (A) $^{\text{CALC}}\text{CCS}_{\text{He}}$ evolution during the desolvation of the 12-d_{66} droplet with -5 net charge. At the top the simulation temperatures are shown along the related trajectory portions. The initial, intermediate, and final structures are shown with DNA strands in cyan, bases aromatic rings in blue, and NH_4^+ cations in orange. On the right the $[12\text{-d}_{66}]^{5\text{-DT}}\text{CCS}_{\text{He}}$ distribution (blue circles) is superimposed on the $^{\text{CALC}}\text{CCS}_{\text{He}}$ (blue area) one. (B) H-bond occupancies of the desolvated helix (right), compared to Watson–Crick H-bond occupancies of a B-helix in solution (left), and to gas-phase B- or A-helices upon unbiased MD in the gas phase (middle). In the B-helix, extra H-bonds form between phosphates across the minor groove; in the A-helix, across the major groove, and in the desolvated helix, across both grooves.

rich DNA duplexes, with one charge every two base pairs, had suggested that A-helices predominate from 8-bp on, and that B-helices are preserved from 18-bp on.^{21,22} To ascertain whether the compaction of lower charge states is a general phenomenon, we measured 12-bp to 36-bp DNA and RNA duplexes, from native solutions, either 100% aqueous or containing sulfolane. The tested duplexes included multiples of d_{66} , r_{66} , d_{100} , and r_{100} , and the DNA duplexes listed as potential CCS calibrants by the Fabris group.³⁶ The results are shown in Figure 5 (experimental values in Supporting Table S3).

We found that DNA and RNA duplexes have very similar gas-phase CCS values, although their helix types differ in solution (B vs A). The theoretical CCS values obtained with unbiased in vacuo MD directly from the solution B-helix are overlaid (B-helix MD trend line in Figure 5). They match only some of the high charge states produced in the presence of sulfolane. However, the low charge states produced from purely aqueous NH_4OAc solutions are significantly more compact.

To reproduce the dual-groove closing of longer duplexes while avoiding computationally costly desolvation simulations, we opted for biased exploration. We used restrained minimization and imposed distance constraints based on our knowledge that compact structures can be formed thanks to hydrogen bonds between phosphates across both grooves. Distance restraints were imposed using a harmonic potential between the hydrogen atom of neutral phosphates belonging to one strand and the oxygen atom of mating phosphates belonging to the other strand (Supporting Information Section S10, Figures S32–S34, and Movie S2 for a 12-bp duplex). The systems were minimized in vacuo, and then all restraints were removed prior to 1- μs gas phase MD.

For 12-bp duplexes, the resulting CCS distributions agree with the experiment, with the strongest compaction for 12-d_{100} (Figure 1E). Applying the same procedure starting from an A-helix however did not lead to similarly low CCS values (Supporting Figure S35). The doubly groove-zipped helices obtained by restrained minimization generally keep WC hydrogen bonds less well than those obtained by desolvation

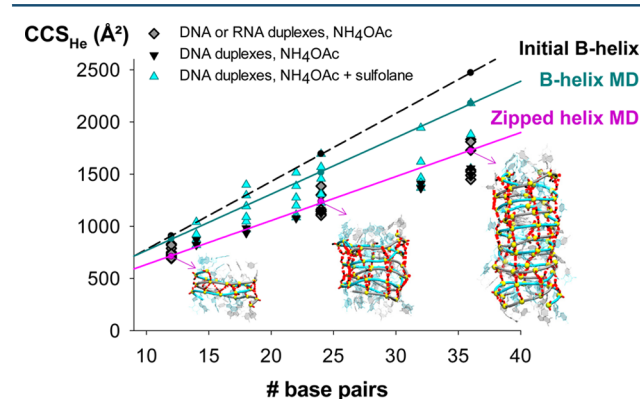


Figure 5. Comparison between experimental and calculated CCS_{He} of 12-bp to 36-bp duplexes. DNA and RNA sequences were either derived from $12\text{-d}/r_{66/100}$ (diamonds, see Tables 2 and S3) or were identical to the DNA duplexes studied by Lippens et al.³⁶ (triangles, see Table S3). When measured at the charge states obtained from aqueous 100-mM NH_4OAc (black and dark gray), collision cross section values match with MD on the zipped helix (restrained minimization followed by MD). DNA duplexes at higher charge states produced by sulfolane addition adopt more extended conformations (cyan), which match better with MD simulations on B-helices.

(Supporting Figure S36–S38), but still reflect the solution trend, with the 12-d₁₀₀ preserving the highest fraction of hydrogen bonds. The advantage of the procedure is to reproduce the phosphate–phosphate H-bond pattern of the desolvated helices (two diagonals for zipping across both grooves, plus the central diagonal indicating preserved base pairs, Figure S36). We then applied restrained minimization to the longer (24-bp and 36-bp) helices (Supporting Figures S39–S40). Whatever the duplex length, the experimental CCS values obtained for low charge states (Figure 5) match better with these zipped helices than with the canonical structures or with the helices relaxed by long unbiased gas-phase MD.

CONCLUSIONS

In summary, at the charge states produced by electrospray from ≥ 100 mM aqueous ammonium acetate (traditional “native” solution conditions), double-stranded nucleic acids undergo a significant compaction in gas phase compared to the structure in solution. Unbiased molecular dynamics of B-helix or A-helix structures directly transposed from solution to the gas phase fails to reproduce the experimental results. This is due to several reasons: (i) only the phosphate groups closest to one another can pair to form hydrogen bonds on the simulation time scale, (ii) the starting structure is unrealistic and (iii) sampling in unbiased MD simulations is intrinsically limited. In the case of T-REMD, depending on the initial choice of charge location, the final structures either did not have any memory of the solution structure, or resembled those obtained by unbiased MD. T-REMD can help to solve the sampling effect (the question of the maximum internal temperature reached in the experiments remaining open), but not the problem that original charge locations might be incorrect.

Gradual desolvation generates more realistic starting structures for gas phase simulations. Conformational transitions occurring during dehydration cannot be ignored because they guide the entire sampling, within a particularly stiff conformational landscape in the case of nucleic acids. The conformationally restrained duplexes remain stable upon unbiased MD: once formed, they stay locked at room temperature. The broadness of the experimental CCS distributions therefore indicates a distribution of coexisting—but not interconverting—conformations, wherein each would have a slightly different phosphate–phosphate hydrogen bond network.

Our results highlight a key difference between nucleic acids and proteins in native mass spectrometry. Globular proteins can rearrange by relaxing their side chains³⁷ and undergo minimal salt bridge rearrangement.³⁸ Briefly optimized structures often have CCS values matching well with the experiments.^{35,39–41} Fabris and co-workers have recently underlined the difficulties in transposing to DNA the MD and CCS calculation protocols traditionally used for proteins.³⁶ As a way out they proposed to calibrate all traveling wave IMS data using short MD simulation results, but our study shows why this approach would lead to a misrepresentation of nucleic acid structures in the gas phase.

DNA and RNA double helices are more compact in the gas phase than in solution, due mostly to new phosphate–phosphate interactions. At the low charge states produced from ammonium acetate, the Coulomb repulsion is not sufficient to keep the phosphate groups apart. They rearrange by self-solvation, cause major rearrangements of the backbone, and lead to a significant compaction (>20%) compared to the starting structure. Yet, they are metastable conformations keeping some memory of the solution structure.

METHODS

Electrospray Ion Mobility Spectrometry. DNA and RNA duplexes were prepared by annealing their corresponding single-strands (purchased from Eurogentec, Seraing, Belgium, with RPartridge-Gold purification) in aqueous 100 mM NH₄OAc. When sprayed at 10 μ M duplex, the major charge states are 4– for the 10-bp, 5– for the 12-bp, 7– for the 24-bp, 8– and 9– for the 36-bp duplexes. Higher charge states were generated by adding 0.2% to 0.75% sulfolane to the solution. ESI-IMS-MS experiments were recorded on an Agilent 6560 IMS-Q-TOF, with the drift tube operated in helium (Supporting Information Section S1). The arrival time distributions were fitted by Gaussian peaks and the CCS values of the center of each peak were determined by the stepped-field method. For visualization, we converted the arrival time distributions into CCS distributions (see Supporting Information).

Gas-Phase Simulations. The starting structures of the duplexes were built with the Nucleic Acid Builder (NAB) software,⁴² both for the A-form (DNA and RNA) and the B-form (DNA). Table 1 lists the main sequences and levels of theory used here. For 12-d₃₃, 12-d₆₆, 12-d₁₀₀ (B-helix), and 12-r₆₆ (A-helix), we first carried out MD simulations in water. Then all water molecules and counterions were removed at once, before each 1- μ s gas-phase simulation. The two possibilities to reduce the total charge to –5 (major charge state) are the localized charges (LC) and distributed charges (DC) models.²⁰ With the LC model, protons are added on 17 out of the 22 phosphate groups. Among the 26 334 possible protonation schemes, we selected a few low-energy ones based on single point molecular mechanics calculations. With the DC model, the net charge of each phosphate group is reduced so that the total charge of the duplex is –5.

Solution and gas phase MD simulations were carried out with the MPI-versions of modules *pmemd* and *sander*, respectively, of the Amber12 suite of programs,⁴³ implementing parmBSC1 force field⁴⁴ for DNA and parmBSC0 force field + χ_{OL3} correction^{45,46} for RNA. The electrostatic interactions were calculated with the particle mesh Ewald algorithm⁴⁷ (real-space cutoff = 10 Å) in solution and direct Coulomb summation (no cutoff) in gas phase. All 12-bp duplexes were subjected gas phase T-REMD⁴⁸ (1 μ s \times 18 replicas) with temperature values from 300.00 to 633.94 K, chosen with predictor from Patriksson et al.⁴⁹ (average successful exchange rate of ca. 30%). Short duplexes (7–10 bp) were optimized at DFT level,⁵⁰ with the M06-2X⁵¹ functional including the dispersion correction GD3.⁵² The basis set was 6-31G(d,p) for the 7–9-bp duplexes (see Supporting Information) and 4–31G(d) for the 10-bp duplex. Duplexes up to 12-bp were also studied at the semiempirical (SE) level with MOPAC,⁵³ using different methods⁵⁴ (further details in Supporting Information). Hydrogen bond and stacking analysis was performed for all simulations as detailed in the Supporting Information Section S4.

Simulation of Desolvation and Proton Transfer. Starting from equilibrated MD simulations in solution, we cut droplets of ca. 2400 water molecules (radius \sim 25 Å) containing the duplex 12-d₆₆, and 16, 17, and 18 NH₄⁺ cations to give a total net charge of –6, –5, and –4, respectively. The droplets were then subjected to gas-phase MD simulations following Koneremann’s protocol.⁵⁵ Briefly, the trajectories were propagated by 500 ps chunks at constant temperature (350 K). To accelerate the evaporation, at the beginning of each chunk the initial velocities were reassigned according to the Boltzmann distribution at $T =$

350 K. At the end of each chunk, we stripped out all water molecules farther than 60 Å from the N6 atom of the 18th residue adenine (which is approximately in the center of the duplex). A further 50 ns chunk at $T = 450$ K helped the last “sticky” water molecules to evaporate. In total, 12 independent trajectories were obtained (four at each charge state, 4−, 5−, and 6−). We then localized the charges (LC model) as follows: on the ultimate conformation of every trajectory a proton from each NH_4^+ cation was transferred to the closest phosphate oxygen atom, and ammonia is removed. The resulting duplexes were then subjected to 1- μs unbiased MD.

CCS Calculations. The collision cross section (CCS) is calculated using the EHSSrot code⁵⁶ with the atom parametrization of Siu et al.,⁵⁷ a combination that is both accurate and efficient for calculating the CCS of nucleic acids in the gas phase.⁵⁸ The CCS is calculated for snapshots every 0.5 ns in each MD trajectory.

■ ASSOCIATED CONTENT

📄 Supporting Information

The Supporting Information is available free of charge on the ACS Publications website at DOI: [10.1021/acscentsci.7b00084](https://doi.org/10.1021/acscentsci.7b00084).

Experimental procedures including reconstruction of the CCS distributions, detailed computational procedures, ESI-IMS-MS supplementary results, circular dichroism results, full modeling results by in vacuo QM optimization, MD, T-REMD, and MD following restrained minimization, structural analysis, supplementary results on longer duplexes, full list of authors for references 43 and 50, and additional references (PDF)

Movie S1: minor groove zipping upon MD of a 12-bp B-helix (AVI)

Movie S2: dual groove zipping imposed by restrained minimization on a 12-bp B-helix (AVI)

■ AUTHOR INFORMATION

Corresponding Author

*Tel: +33 (0)5 4000 2940. E-mail: v.gabelica@iecb.u-bordeaux.fr.

ORCID

Modesto Orozco: [0000-0002-8608-3278](https://orcid.org/0000-0002-8608-3278)

Valérie Gabelica: [0000-0001-9496-0165](https://orcid.org/0000-0001-9496-0165)

Notes

The authors declare no competing financial interest.

■ ACKNOWLEDGMENTS

This work was funded by the European Research Council (ERC DNFOLDIMS to V.G. and ERC SimDNA to M.O.), by the Spanish BIO2015-69802-R grant to MO, and by EU COST action BM1403 (short-term scientific mission to MP). HG is a Juan de la Cierva researcher. LD is a SNI (Sistema Nacional de Investigadores; ANII, Uruguay) researcher, and MO is an ICREA-academia fellow. We are thankful to David E. Condon for donating to us the Perl script used to score the base stacking, and to Adrien Marchand and members of COST action BM1403 for fruitful discussions.

■ REFERENCES

- (1) Blackburn, G. M.; Gait, M. J. *Nucleic Acids in Chemistry and Biology*; Oxford University Press: Oxford, 1996.
- (2) Rhodes, D.; Lipps, H. J. G-quadruplexes and their regulatory roles in biology. *Nucleic Acids Res.* **2015**, *43*, 8627–8637.

- (3) Breaker, R. R. Prospects for riboswitch discovery and analysis. *Mol. Cell* **2011**, *43*, 867–879.

- (4) Loo, J. A. Studying non-covalent protein complexes by electrospray ionization mass spectrometry. *Mass Spectrom. Rev.* **1997**, *16*, 1–23.

- (5) Breuker, K. The study of protein–ligand interactions by mass spectrometry—a personal view. *Int. J. Mass Spectrom.* **2004**, *239*, 33–41.

- (6) Rosu, F.; De Pauw, E.; Gabelica, V. Electrospray mass spectrometry to study drug–nucleic acids interactions. *Biochimie* **2008**, *90*, 1074–1087.

- (7) Kitova, E. N.; El-Hawiet, A.; Schnier, P. D.; Klassen, J. S. Reliable determinations of protein–ligand interactions by direct ESI-MS measurements. Are we there yet? *J. Am. Soc. Mass Spectrom.* **2012**, *23*, 431–441.

- (8) Leney, A. C.; Heck, A. J. R. Native Mass Spectrometry: What is in the Name? *J. Am. Soc. Mass Spectrom.* **2017**, *28*, 5–13.

- (9) Bohrer, B. C.; Merenbloom, S. I.; Koeniger, S. L.; Hilderbrand, A. E.; Clemmer, D. E. Biomolecule analysis by ion mobility spectrometry. *Annu. Rev. Anal. Chem.* **2008**, *1*, 293–327.

- (10) Uetrecht, C.; Rose, R. J.; van Duijn, E.; Lorenzen, K.; Heck, A. J. Ion mobility mass spectrometry of proteins and protein assemblies. *Chem. Soc. Rev.* **2010**, *39*, 1633–1655.

- (11) Zheng, X.; Liu, D.; Klarner, F. G.; Schrader, T.; Bitan, G.; Bowers, M. T. Amyloid beta-protein assembly: The effect of molecular tweezers CLR01 and CLR03. *J. Phys. Chem. B* **2015**, *119*, 4831–4841.

- (12) Canon, F.; Ballivian, R.; Chirot, F.; Antoine, R.; Sarni-Manchado, P.; Lemoine, J.; Dugourd, P. Folding of a salivary intrinsically disordered protein upon binding to tannins. *J. Am. Chem. Soc.* **2011**, *133*, 7847–7852.

- (13) Hyung, S. J.; Robinson, C. V.; Ruotolo, B. T. Gas-phase unfolding and disassembly reveals stability differences in ligand-bound multi-protein complexes. *Chem. Biol.* **2009**, *16*, 382–390.

- (14) Ujma, J.; De Cecco, M.; Chepelin, O.; Levene, H.; Moffat, C.; Pike, S. J.; Lusby, P. J.; Barran, P. E. Shapes of supramolecular cages by ion mobility mass spectrometry. *Chem. Commun.* **2012**, *48*, 4423–4425.

- (15) Schnier, P. D.; Klassen, J. S.; Strittmatter, E. F.; Williams, E. R. Activation energies for dissociation of double strand oligonucleotide anions: evidence for Watson–Crick base pairing in vacuo. *J. Am. Chem. Soc.* **1998**, *120*, 9605–9613.

- (16) Gabelica, V.; De Pauw, E. Collision-Induced Dissociation of 16-mer DNA Duplexes with Various Sequences: Evidence for Conservation of the Double Helix Conformation in the Gas Phase. *Int. J. Mass Spectrom.* **2002**, *219*, 151–159.

- (17) Pan, S.; Sun, X. J.; Lee, J. K. Stability of complementary and mismatched DNA duplexes: Comparison and contrast in gas versus solution phases. *Int. J. Mass Spectrom.* **2006**, *253*, 238–248.

- (18) Burmistrova, A.; Gabelica, V.; Duwez, A. S.; De Pauw, E. Ion mobility spectrometry reveals duplex DNA dissociation intermediates. *J. Am. Soc. Mass Spectrom.* **2013**, *24*, 1777–1786.

- (19) Gabelica, V.; Rosu, F. Gas-Phase Spectroscopy of Nucleic Acids. In *Nucleic Acids in the Gas Phase*; Gabelica, V., Ed.; Springer: Berlin, 2014; pp 103–130.

- (20) Rueda, M.; Kalko, S. G.; Luque, F. J.; Orozco, M. The structure and dynamics of DNA in the gas phase. *J. Am. Chem. Soc.* **2003**, *125*, 8007–8014.

- (21) Gidden, J.; Ferzoco, A.; Baker, E. S.; Bowers, M. T. Duplex formation and the onset of helicity in poly d(CG)n oligonucleotides in a solvent-free environment. *J. Am. Chem. Soc.* **2004**, *126*, 15132–15140.

- (22) Baker, E. S.; Bowers, M. T. B-DNA helix stability in a solvent-free environment. *J. Am. Soc. Mass Spectrom.* **2007**, *18*, 1188–1195.

- (23) Drew, H.; Wing, R.; Takano, T.; Broka, C.; Tanaka, S.; Itakura, K.; Dickerson, R. E. Structure of B-DNA dodecamer: conformation and dynamics. *Proc. Natl. Acad. Sci. U. S. A.* **1981**, *78*, 2179–2183.

- (24) Kypr, J.; Kejnovska, I.; Renciuik, D.; Vorlickova, M. Circular dichroism and conformational polymorphism of DNA. *Nucleic Acids Res.* **2009**, *37*, 1713–1725.

- (25) Lipfert, J.; Doniach, S.; Das, R.; Herschlag, D. Understanding nucleic acid–ion interactions. *Annu. Rev. Biochem.* **2014**, *83*, 813–841.

- (26) Pasi, M.; Maddocks, J. H.; Lavery, R. Analyzing ion distributions around DNA: sequence-dependence of potassium ion distributions

from microsecond molecular dynamics. *Nucleic Acids Res.* **2015**, *43*, 2412–2423.

(27) Manning, G. S. The molecular theory of polyelectrolyte solutions with applications to the electrostatic properties of polynucleotides. *Q. Rev. Biophys.* **1978**, *11*, 179–246.

(28) Ogorzalek Loo, R. R.; Lakshmanan, R.; Loo, J. A. What protein charging (and supercharging) reveal about the mechanism of electro-spray ionization. *J. Am. Soc. Mass Spectrom.* **2014**, *25*, 1675–1693.

(29) Humphrey, W.; Dalke, A.; Schulten, K. VMD: visual molecular dynamics. *J. Mol. Graphics* **1996**, *14*, 33–38.

(30) Zubatiuk, T.; Kukuev, M. A.; Korolyova, A. S.; Gorb, L.; Nyporko, A.; Hovorun, D.; Leszczynski, J. Structure and Binding Energy of Double-Stranded A-DNA Mini-helices: Quantum-Chemical Study. *J. Phys. Chem. B* **2015**, *119*, 12741–12749.

(31) Zubatiuk, T. A.; Shishkin, O. V.; Gorb, L.; Hovorun, D. M.; Leszczynski, J. B-DNA characteristics are preserved in double stranded d(A)₃d(T)₃ and d(G)₃d(C)₃ mini-helices: conclusions from DFT/M06-2X study. *Phys. Chem. Chem. Phys.* **2013**, *15*, 18155–18166.

(32) Condon, D. E.; Kennedy, S. D.; Mort, B. C.; Kierzek, R.; Yildirim, I.; Turner, D. H. Stacking in RNA: NMR of Four Tetramers Benchmark Molecular Dynamics. *J. Chem. Theory Comput.* **2015**, *11*, 2729–2742.

(33) Sharawy, M.; Consta, S. How do non-covalent complexes dissociate in droplets? A case study of the desolvation of dsDNA from a charged aqueous nanodrop. *Phys. Chem. Chem. Phys.* **2015**, *17*, 25550–25562.

(34) Dole, M.; Mack, L. L.; Hines, R. L.; Mobley, R. C.; Ferguson, L. D.; Alice, M. B. Molecular beams of macroions. *J. Chem. Phys.* **1968**, *49*, 2240–2249.

(35) McAllister, R. G.; Metwally, H.; Sun, Y.; Konermann, L. Release of Native-like Gaseous Proteins from Electrospray Droplets via the Charged Residue Mechanism: Insights from Molecular Dynamics Simulations. *J. Am. Chem. Soc.* **2015**, *137*, 12667–12676.

(36) Lippens, J. L.; Ranganathan, S. V.; D'Esposito, R. J.; Fabris, D. Modular calibrant sets for the structural analysis of nucleic acids by ion mobility spectrometry mass spectrometry. *Analyst* **2016**, *141*, 4084–4099.

(37) Breuker, K.; McLafferty, F. W. Stepwise evolution of protein native structure with electrospray into the gas phase, 10⁻¹² to 10² s. *Proc. Natl. Acad. Sci. U. S. A.* **2008**, *105*, 18145–18152.

(38) Loo, R. R.; Loo, J. A. Salt Bridge Rearrangement (SaBRe) Explains the Dissociation Behavior of Noncovalent Complexes. *J. Am. Soc. Mass Spectrom.* **2016**, *27*, 975–990.

(39) Pacholarz, K. J.; Porrini, M.; Garlish, R. A.; Burnley, R. J.; Taylor, R. J.; Henry, A. J.; Barran, P. E. Dynamics of intact immunoglobulin G explored by drift-tube ion-mobility mass spectrometry and molecular modeling. *Angew. Chem., Int. Ed.* **2014**, *53*, 7765–7769.

(40) Meyer, T.; de la Cruz, X.; Orozco, M. An atomistic view to the gas phase proteome. *Structure* **2009**, *17*, 88–95.

(41) Harvey, S. R.; Porrini, M.; Konijnenberg, A.; Clarke, D. J.; Tyler, R. C.; Langridge-Smith, P. R.; MacPhee, C. E.; Volkman, B. F.; Barran, P. E. Dissecting the dynamic conformations of the metamorphic protein lymphotactin. *J. Phys. Chem. B* **2014**, *118*, 12348–12359.

(42) Macke, T.; Case, D. A. Modeling unusual nucleic acid structures. In *Molecular Modeling of Nucleic Acids*; Leontes, N. B., Santa Lucia, J., Jr., Eds.; American Chemical Society: Washington, DC, 1998; pp 379–393.

(43) Case, D. A., et. al. *AMBER 12*; University of California: San Francisco, 2012.

(44) Ivani, I.; Dans, P. D.; Noy, A.; Perez, A.; Faustino, I.; Hospital, A.; Walther, J.; Andrio, P.; Goni, R.; Balaceanu, A.; Portella, G.; Battistini, F.; Gelpi, J. L.; Gonzalez, C.; Vendruscolo, M.; Loughton, C. A.; Harris, S. A.; Case, D. A.; Orozco, M. Parmbsc1: a refined force field for DNA simulations. *Nat. Methods* **2016**, *13*, 55–58.

(45) Perez, A.; Marchan, I.; Svozil, D.; Sponer, J.; Cheatham, T. E., 3rd; Loughton, C. A.; Orozco, M. Refinement of the AMBER force field for nucleic acids: improving the description of alpha/gamma conformers. *Biophys. J.* **2007**, *92*, 3817–3829.

(46) Zgarbova, M.; Otyepka, M.; Sponer, J.; Mladek, A.; Banas, P.; Cheatham, T. E., 3rd; Jurecka, P. Refinement of the Cornell et al. Nucleic Acids Force Field Based on Reference Quantum Chemical

Calculations of Glycosidic Torsion Profiles. *J. Chem. Theory Comput.* **2011**, *7*, 2886–2902.

(47) Darden, T.; York, D.; Pedersen, L. Particle mesh Ewald: An N·log(N) method for Ewald sums in large systems. *J. Chem. Phys.* **1993**, *98*, 10089.

(48) Sugita, Y.; Okamoto, Y. Replica-exchange molecular dynamics method for protein folding. *Chem. Phys. Lett.* **1999**, *314*, 141–151.

(49) Patriksson, A.; van der Spoel, D. A temperature predictor for parallel tempering simulations. *Phys. Chem. Chem. Phys.* **2008**, *10*, 2073–2077.

(50) Frisch, M. J., et. al. *Gaussian 09*; Gaussian, Inc.: Wallingford, CT, USA, 2009.

(51) Zhao, Y.; Truhlar, D. G. The M06 suite of density functionals for main group thermochemistry, thermochemical kinetics, noncovalent interactions, excited states, and transition elements: two new functionals and systematic testing of four M06-class functionals and 12 other functionals. *Theor. Chem. Acc.* **2008**, *120*, 215–241.

(52) Grimme, S.; Antony, J.; Ehrlich, S.; Krieg, H. A consistent and accurate ab initio parametrization of density functional dispersion correction (DFT-D) for the 94 elements H-Pu. *J. Chem. Phys.* **2010**, *132*, 154104.

(53) Stewart, J. J. P. *MOPAC2012: Stewart Computational Chemistry*; Colorado Springs, CO, USA, 2012.

(54) Stewart, J. J. Optimization of parameters for semiempirical methods VI: more modifications to the NDDO approximations and re-optimization of parameters. *J. Mol. Model.* **2013**, *19*, 1–32.

(55) Metwally, H.; McAllister, R. G.; Konermann, L. Exploring the mechanism of salt-induced signal suppression in protein electrospray mass spectrometry using experiments and molecular dynamics simulations. *Anal. Chem.* **2015**, *87*, 2434–2442.

(56) Shvartsburg, A. A.; Mashkevich, S. V.; Baker, E. S.; Smith, R. D. Optimization of algorithms for ion mobility calculations. *J. Phys. Chem. A* **2007**, *111*, 2002–2010.

(57) Siu, C. K.; Guo, Y.; Saminathan, I. S.; Hopkinson, A. C.; Siu, K. W. Optimization of parameters used in algorithms of ion-mobility calculation for conformational analyses. *J. Phys. Chem. B* **2010**, *114*, 1204–1212.

(58) D'Atri, V.; Porrini, M.; Rosu, F.; Gabelica, V. Linking molecular models with ion mobility experiments. Illustration with a rigid nucleic acid structure. *J. Mass Spectrom.* **2015**, *50*, 711–726.